

EVALUATION OF THE POUNDING FORCES DURING EARTHQUAKE USING EXPLICIT DYNAMIC TIME INTEGRATION METHOD

George Bogdan NICA – Assistant professor, PhD, Technical University of Civil Engineering,
e-mail: george.nica@utcb.ro

Andrei Gheorghe PRICOPIE – Lecturer, PhD, Technical University of Civil Engineering,
e-mail: andrei.pricopie@gmail.com

Abstract: Pounding effects during earthquake is a subject of high significance for structural engineers performing in the urban areas. In this paper, two ways to account for structural pounding are used in a MATLAB code, namely classical stereomechanics approach and nonlinear viscoelastic impact element. The numerical study is performed on SDOF structures acted by EL-Centro recording. While most of the studies available in the literature are related to Newmark implicit time integration method, in this study the equations of motion are numerical integrated using central finite difference method, an explicit method, having the main advantage that in the displacement at the $i^{\text{th}}+1$ step is calculated based on the loads from the i^{th} step. Thus, the collision is checked and the pounding forces are taken into account into the equation of motion in an easier manner than in an implicit integration method. First, a comparison is done using available data in the literature. Both linear and nonlinear behavior of the structures during earthquake is further investigated. Several layout scenarios are also investigated, in which one or more weak buildings are adjacent to a stiffer building. One of the main findings in this paper is related to the behavior of a weak structure located between two stiff structures.

Keywords: SDOF, stereomechanics, nonlinear viscoelastic, gap

1. Introduction

In the past decades the number of buildings increased rapidly to fulfill the human needs. Most of the new structures are tall buildings, constructed in close proximity to other. During seismic actions a new problem arises in such cases, namely pounding of adjacent buildings, which consists of collisions at different levels due the different dynamic characteristics. The repeated impulsive actions cause additional internal resultants, which are not taken into account in the common design process.

The pounding phenomenon idealization is usually studied using single degree of freedom (SDOF) or multi degree of freedom (MDOF) models, in which the mass of each storey is considered lumped. One of the first of such analysis is the study of Anagnostopoulos [1], and recent work is the studies of Mate et al. [2],[3], the studies of Jankowski [4-7] and the study of S.A. Salam [8]. The study of Barros [9] shows the benefit of equipping the structures with shear walls to protect structures against pounding effects. The study of Polycarpou [10] presents an efficient methodology for the numerical simulation of pounding of adjacent buildings in 3D, in which a force-based impact model is proposed. Collision of structural elements has been studied also using finite element codes [11]-[14], in which different types of 2D or 3D structures are analyzed with different software. Applied element method, a numerical method in which the elements are connected by nonlinear springs, has been used by Ehab et. al. [15], to study structural pounding.

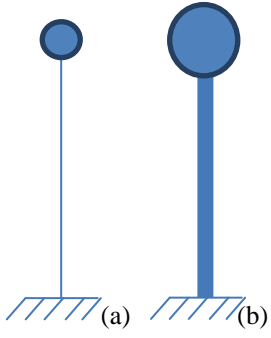
In this paper, two idealized SDOF structures are acted by El-Centro recording and their linear and non-linear response is obtained using an explicit code developed in MATLAB. The pounding forces between these two structures are evaluated both by using the classical stereomechanics approach and using nonlinear viscoelastic model. The numerical data is compared in terms of forces, collision time and total transferred momentum. Finally, several layouts of three structures with different dynamic characteristics are proposed and analyzed.

2. Linear and non-linear seismic response of the reference SDOF structures

In this chapter the seismic response of two structures is obtained, in order to validate and compare the results in the subsequent chapters. The two structures are considered first independent, namely no contact arises between the structures. The data for the two structures are consistent with the data available in [7], to which a elastoplastic with yield deformation force-deformation relation is added. The data is tabulated in table 1. The damping coefficient is proportional to the mass and stiffness (Rayleigh damping). The linear elastic time histories under the first 10 s of the NS component of the El Centro recording for both structures are plotted in Fig. 2a, while the nonlinear response are plotted in Fig. 2b.

Table 1

Dynamic characteristics of the reference structures

	Reference weak structure (a)	Reference stiff structure (b)	
Mass (kg)	75000	3000000	
Stiffness coefficient (kN/m)	2056	1316000	
Natural period (s)	1.2	0.3	
Damping ratio	0.05	0.05	
Yield force (kN)	70	4000	
Yield deformation (m)	0.034	0.003	

The time integration method is the central difference method. The time derivatives \dot{u}_i, \ddot{u}_i are approximated using constant time steps Δt and replaced in the SDOF i^{th} equation of motion (1). The terms are rearranged to obtain the $i^{\text{th}+1}$ displacement u (2), as a function of previous displacements u_{i-1}, u_i , initial dynamic characteristics m, c, k , time step Δt , and i^{th} load p_i .

$$m \frac{u_{i+1} - 2u_i + u_{i-1}}{(\Delta t)^2} + c \frac{u_{i+1} - u_{i-1}}{2\Delta t} + ku_i = p_i \leftrightarrow \quad (1)$$

$$\left[\frac{m}{(\Delta t)^2} + \frac{c}{2\Delta t} \right] u_{i+1} = p_i - \left[\frac{m}{(\Delta t)^2} - \frac{c}{2\Delta t} \right] u_{i-1} - \left[k - \frac{2m}{(\Delta t)^2} \right] u_i \quad (2)$$

An advantage of the central difference method is that it can be easily adapted for solving nonlinear equation of motion. Replacing ku_i with resisting force $(f_s)_i$ one will obtain equation (3). Thus, the resisting force appears explicitly, as it depends on the displacement at time i , not on the unknown displacement at time $i+1$ [16].

$$\left[\frac{m}{(\Delta t)^2} + \frac{c}{2\Delta t} \right] u_{i+1} = p_i - \left[\frac{m}{(\Delta t)^2} - \frac{c}{2\Delta t} \right] u_{i-1} + \frac{2m}{(\Delta t)^2} u_i - (f_s)_i \quad (3)$$

The specific requirement for stability is $T_n > \pi\Delta t$, but this is never a constraint in SDOF systems because a smaller step is usually chosen to obtain accurate results [16]. In this paper, the timestep chosen is 0.01 s.

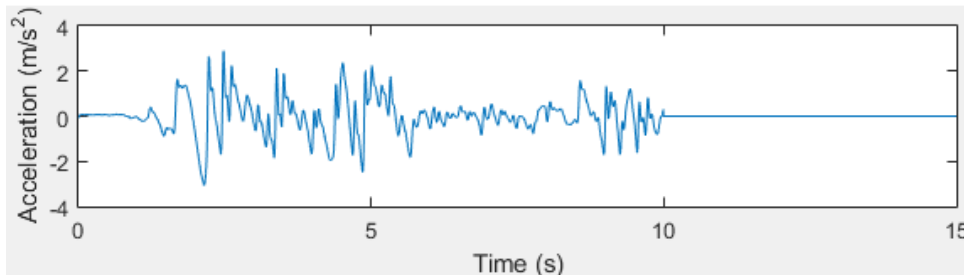


Fig. 1 - First 10s of NS component of El Centro Recording used in this paper

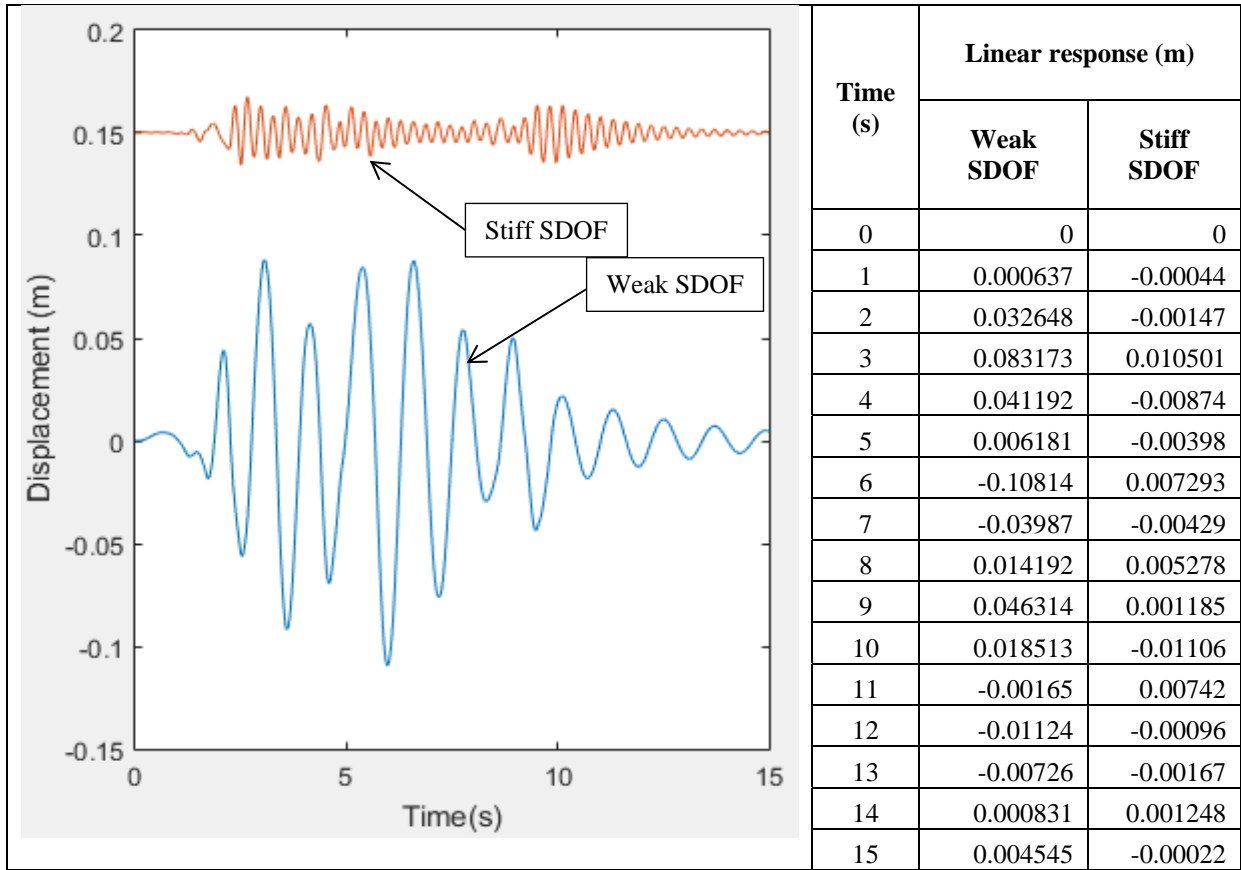


Fig. 2a - Linear elastic time histories under the first 10 s of the NS component of the El Centro recording for both SDOF's

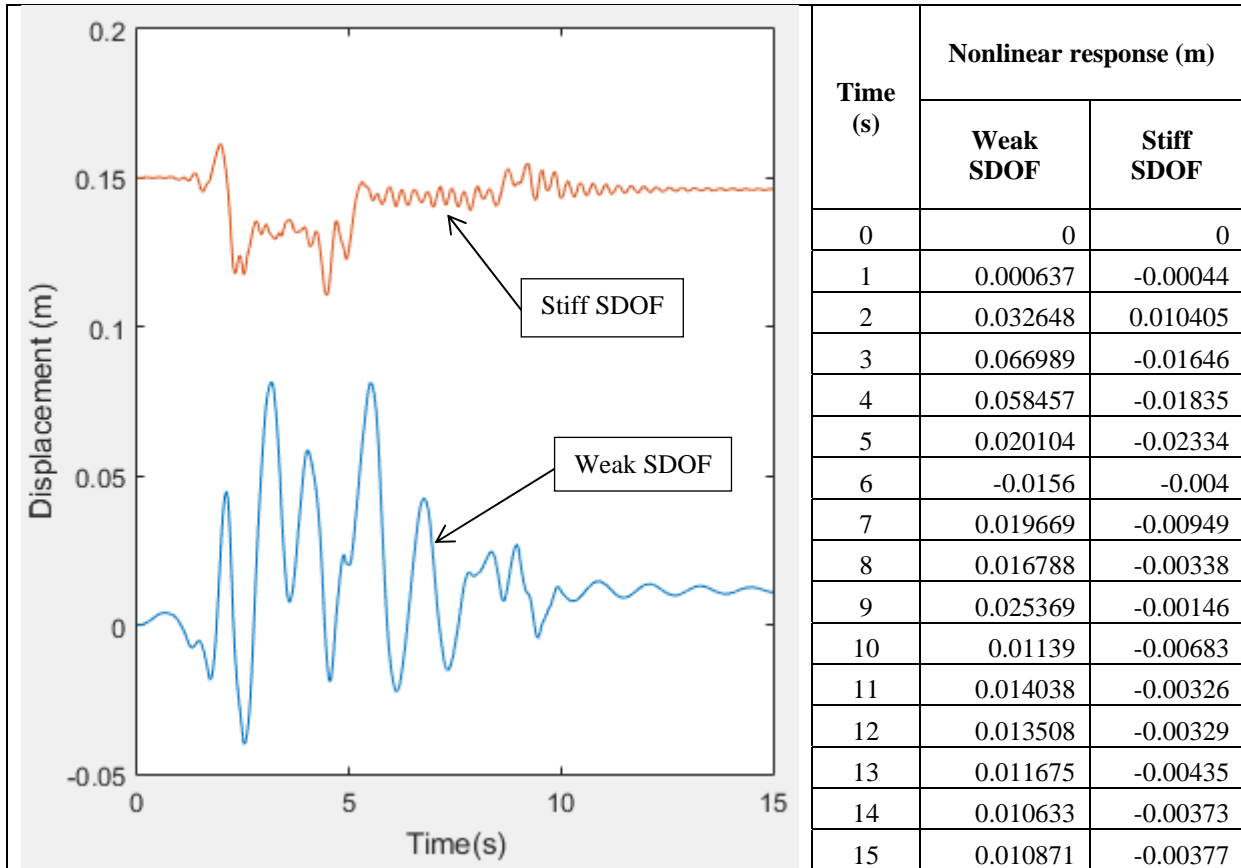


Fig. 2b - Nonlinear time histories under the first 10 s of the NS component of the El Centro recording for both SDOF's

3. Structural pounding between two adjacent structures

In this chapter the stereomechanics approach is employed and compared with the data obtained using nonlinear viscoelastic impact element. The two structures are considered to be in the close proximity. In order to validate the data, the gap distance equal to 3 cm is used, as it was used in [7], the major difference being the time integration method and the comparison with the stereomechanics approach.

3.1. Linear and nonlinear response using stereomechanics approach

The classical theory of impact is based primarily on the momentum law for rigid bodies. Due to its mathematical simplicity, it is incapable of describing transient stresses, forces or deformations. The theory fails to account for local deformations at the contact point. For perfectly elastic impact of two bodies, the conservation of energy law provides the second relation required to uniquely determine the final velocities of the objects [17]. Permanent deformations are considered if a restitution coefficient e , defined as the ratio of final to initial relative velocity components of striking objects, is used. Equation (4) presents the conservation of linear momentum and conservation of kinetic energy, for central impact of two colliding bodies. One may observe that, for $e = 1$, the equation reduces to classic mechanics in which no energy loss is considered, while for $e = 0$ completely plastic impact is considered.

$$\begin{aligned}
 & \begin{cases} m_1 v_1^0 + m_2 v_2^0 = m_1 v_1^F + m_2 v_2^F \\ \frac{m_1 (v_1^0)^2}{2} + \frac{m_2 (v_2^0)^2}{2} = \frac{m_1 (v_1^F)^2}{2} + \frac{m_2 (v_2^F)^2}{2} \end{cases} \\
 & \Leftrightarrow \begin{cases} v_1^F = v_1^0 - 2 \frac{m_2 v_1^0 - m_2 v_2^0}{m_1 + m_2} \\ v_2^F = v_2^0 + 2 \frac{m_1 v_1^0 - m_1 v_2^0}{m_1 + m_2} \end{cases} \quad (4) \\
 & \Leftrightarrow \begin{cases} v_1^F = v_1^0 - (1 + e) \frac{m_2 v_1^0 - m_2 v_2^0}{m_1 + m_2} \\ v_2^F = v_2^0 + (1 + e) \frac{m_1 v_1^0 - m_1 v_2^0}{m_1 + m_2} \end{cases} \Leftrightarrow \text{where } e \\
 & = \frac{v_2^F - v_1^F}{v_1^0 - v_2^0}
 \end{aligned}$$

The value of e is determined experimentally by dropping a sphere from a height on a massive plate, both made of the same material. The recorded rebound height is measured, and e is calculated as the square root of the ratio of the initial to the rebound height [17]. In this paper, the value of restitution coefficient is considered 0.65 [17]. On each time step the $i^{\text{th}}+1$ displacement is calculated and the possibility of collision is checked. If the collision will exist, the magnitude of the change of momentum as the product of relative velocity times the mass is calculated. The momentum is divided by the timestep to obtain the pounding forces, and finally the pounding forces are added to the equation of motion in the $i^{\text{th}}+1$ time step.

Fig. 3 illustrates the time and impact forces for the gap considered. The transferred momentum, calculated as the area under the impact forces time history, is estimated as $H_{lin}^{stereo} = 338.86 \text{ kN} \cdot \text{s}$ for the case of linear response, and $H_{nonlin}^{stereo} = 31.653 \text{ kN} \cdot \text{s}$, in the case of non-linear response. Table 2 presents the time (s) and value of pounding forces for the two colliding SDOF structures. The observation is that the first collision is almost at the same time and almost the same magnitude of pounding force is obtained, either considering elastic or

nonlinear behavior. Fig. 4 illustrates the displacement time history and impact forces in the case of nonlinear response.

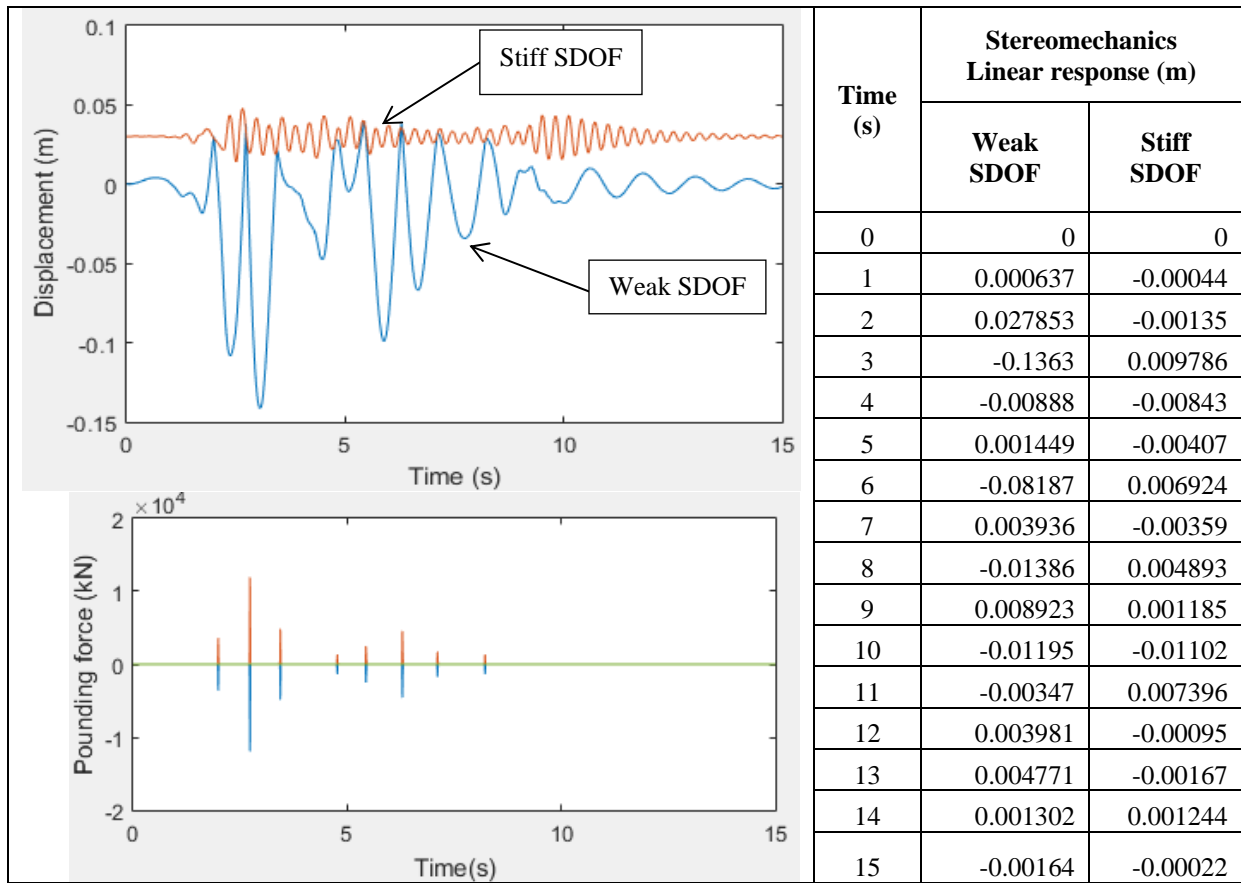


Fig. 3 - Stereomechanical impact: linear elastic time histories under the first 10 s of the NS component of the El Centro recording for both SDOF's

Table 2

Pounding forces estimation in the case of considering stereomechanical impact.

Time (s)	Elastic response: Pounding force [kN]		Time (s)	Nonlinear response: Pounding force [kN]	
	Pounding force for weak SDOF	Pounding force for Stiff SDOF		Pounding force for weak SDOF	Pounding force for Stiff SDOF
1.99	-3607.14	3607.137	2.03	-3165.286	3165.286
2.73	-11917.9	11917.91	No other collisions		
3.44	-4858.64	4858.638			
4.77	-1357.6	1357.603			
5.44	-2485.76	2485.756			
5.45	-792.455	792.4547			
6.29	-4575.56	4575.559			
6.3	-956.605	956.6048			
7.11	-1717.35	1717.346			
7.12	-245.551	245.5509			
8.22	-1371.53	1371.529			

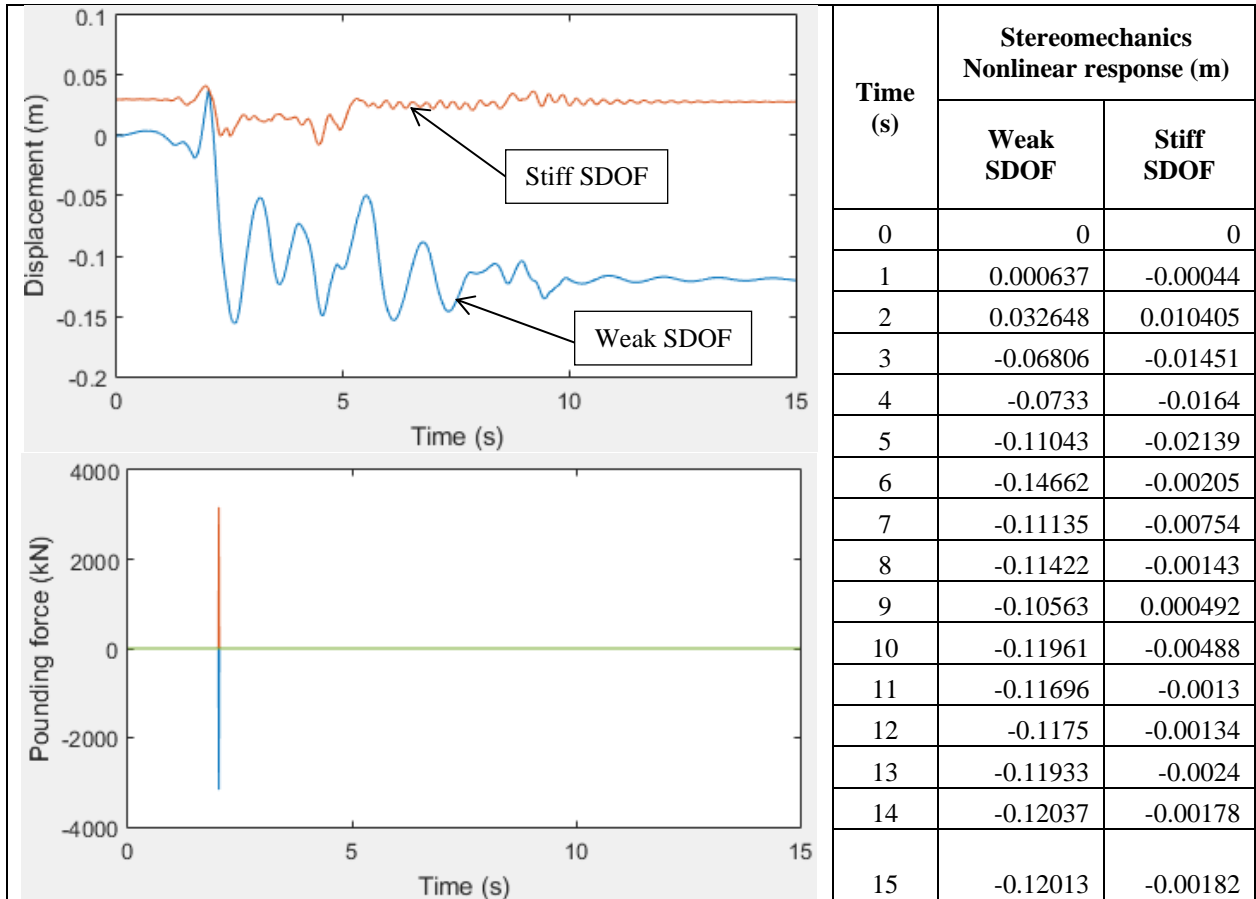


Fig. 4 - Stereomechanical impact: Nonlinear time histories under the first 10 s of the NS component of the El Centro recording for both SDOF's

3.2. Linear and nonlinear response using nonlinear viscoelastic impact element approach

The experimental results [7], [17] show that the pounding force history depends not only on mass, but also on the surface geometry, material properties, prior velocities and material history. Two periods are defined during impact: approach period, starting at the beginning of contact and lasting until the peak deformation, and restitution period [7],[17]. The pounding force time history and energy loss are not symmetric in these two periods: on the approach period a rapid increase in pounding force is observed and majority of energy is dissipated, while on the restitution period the pounding forces decrease with a lower rate and small amount of energy is dissipated [7], [17]. In this paper, the nonlinear viscoelastic impact element is used and the data is compared with the corresponding values obtained in the stereomechanical approach, and also with the available data in literature. Table 3 summarizes the pounding forces during approach period $F^a(t)$ and restitution period $F^r(t)$, and $\delta(t)$ represents the deformation of colliding structural elements.

Table 3

Expression of the pounding forces in the nonlinear viscoelastic model [7]

	$F^a(t) = \bar{\beta}\delta^3(t) + \bar{c}(t)\dot{\delta}(t)$ $\bar{c}(t) = 2\bar{\xi}\sqrt{\bar{\beta}}\sqrt{ \dot{\delta}(t) }\frac{m_1m_2}{m_1+m_2}$	<p>Approach period</p>
	$F^r(t) = \bar{\beta}\delta^3(t)$	<p>Restitution period</p>

The parameters for the nonlinear viscoelastic model are taken from [7], i.e. $\bar{\beta} = 2.75 \times 10^6 \text{ kN/m}^{1.5}$ and $\bar{\xi} = f(e) = 0.35$. Fig. 5 illustrates the time and impact forces for the 3 cm gap considered. The transferred momentum, calculated as the area under the impact forces time history, is estimated as $H_{lin}^{nonlin visco} = 381.49 \text{ kN} \cdot \text{s}$ for the case of linear response, and $H_{nonlin}^{nonlin visco} = 24.35 \text{ kN} \cdot \text{s}$, in the case of non-linear response. Table 4 presents the value of pounding forces vs. time (s) for the two colliding SDOF structures. The observation is that the first collision is almost at the same time and almost the same magnitude of transferred momentum is obtained, either considering elastic or nonlinear behavior. Fig. 6 illustrates the displacement time history and impact forces in the case of nonlinear response.

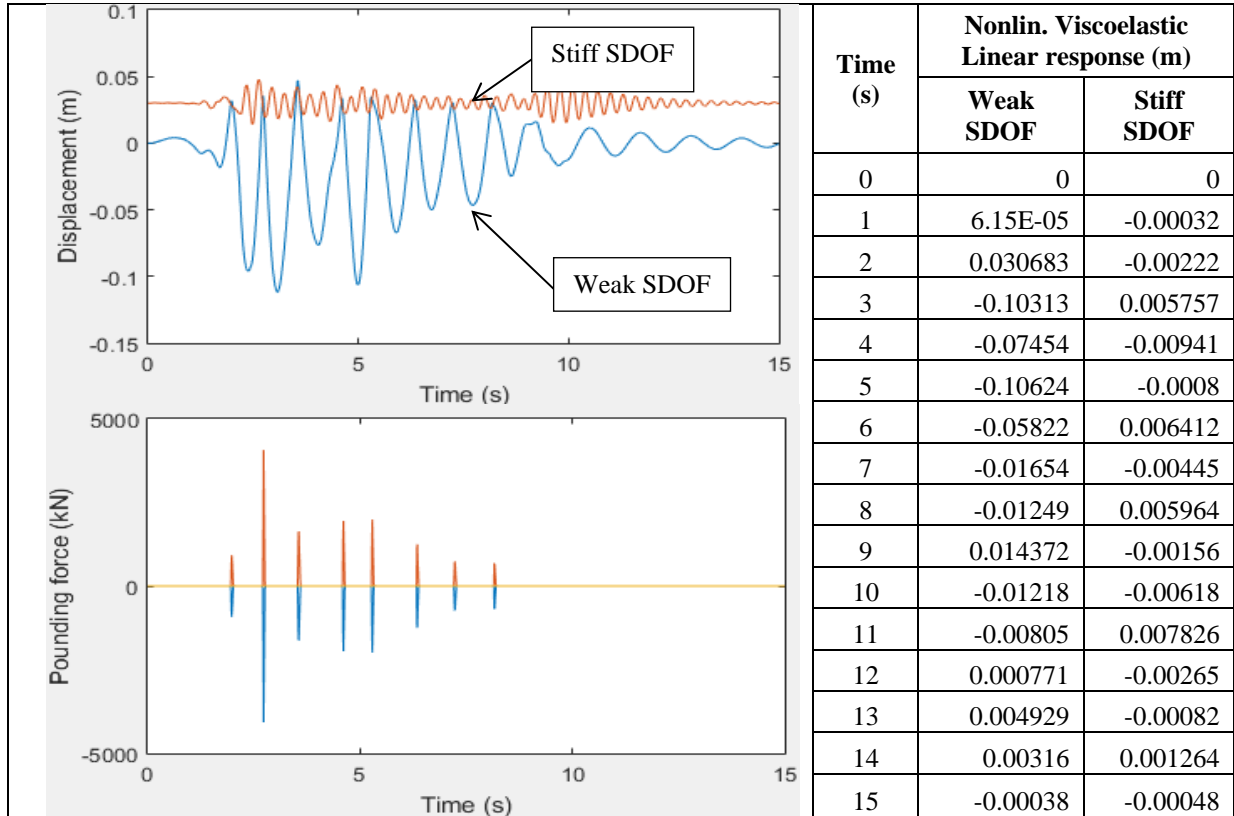


Fig. 5 - Nonlinear viscoelastic impact element: linear elastic time histories under the first 10 s of the NS component of the El Centro recording for both SDOF's

Table 4

Pounding forces in the case of considering nonlinear viscoelastic impact element.

Time (s)		Elastic response: Pounding force [kN]		Time (s)	Nonlinear response: Pounding force [kN]	
		Pounding force for weak SDOF	Pounding force for Stiff SDOF		Pounding force for weak SDOF	Pounding force for Stiff SDOF
First collision	1.97	-677.47	677.4704	2.01	-286.803	286.8025
	1.98	-921.945	921.9447	2.02	-739.887	739.8866
	1.99	-696.302	696.3021	2.03	-710.048	710.0481
	2	-429.418	429.4177	2.04	-442.349	442.3487
	2.01	-152.277	152.2768	2.05	-235.031	235.0306
Second collision	2.72	-1583.89	1583.894	2.06	-20.8271	20.82713
	2.73	-4070.12	4070.12	Second collision, as illustrated in figure 5.		
	2.74	-2909.24	2909.243			
	2.75	-1421.82	1421.817			
	2.76	-122.202	122.2019			

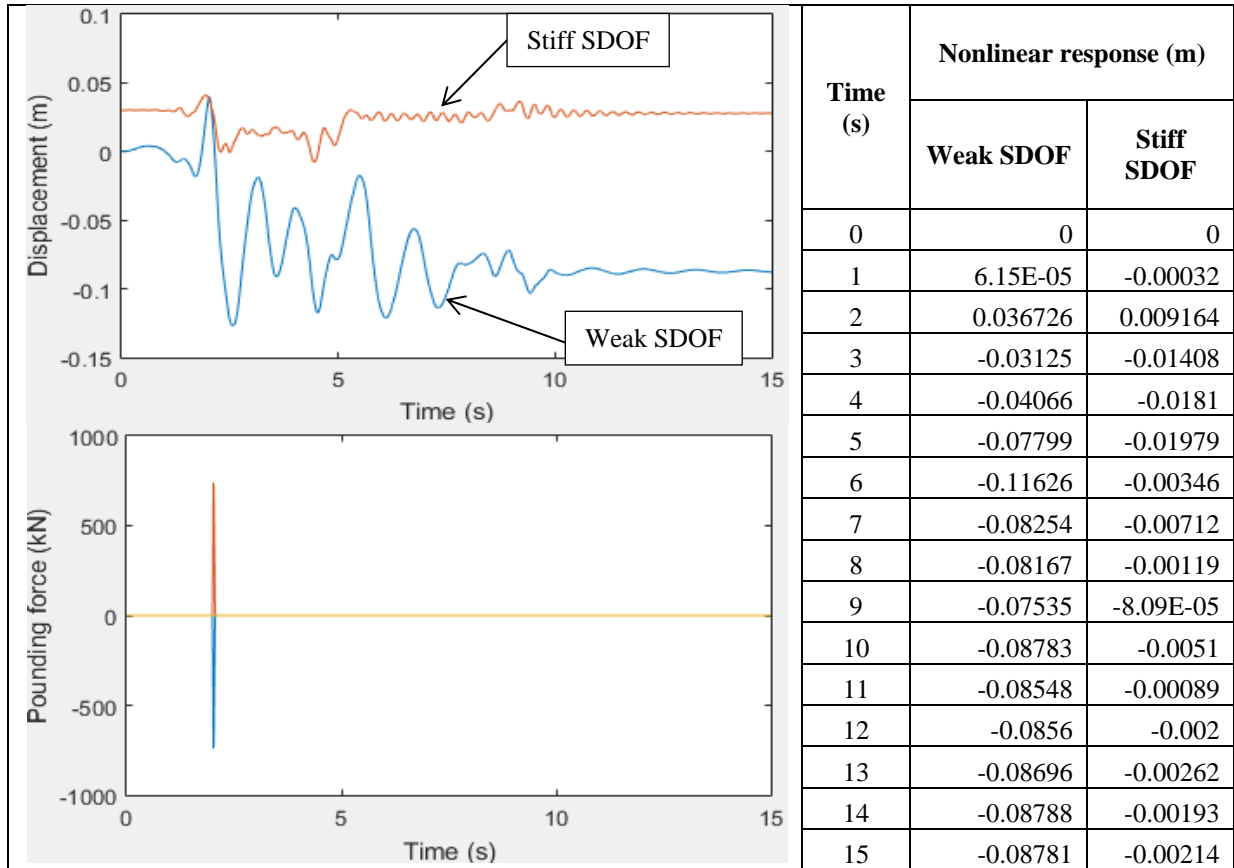


Fig. 6 - Nonlinear viscoelastic impact element: Nonlinear time histories under the first 10 s of the NS component of the El Centro recording for both SDOF's

3.3. Comparison between the analyzed models

The four previously analyzed scenarios are compared in terms of number of collisions, collision time, pounding force and transferred momentum. First, the models considering linear behavior of the SDOF are compared and validated with the corresponding values illustrated in figure 3.1, page 37 of reference [7]. The same number of collisions and collision time are obtained in reference [7] considering Newmark time integration method ($\Delta t = 0.005$ s), whereas the pounding forces in the first and second collision are estimated at nearly 1800 kN and 5400 kN, respectively. No information related to the transferred momentum is given in reference [7]. The corresponding model – linear behavior of the structure and pounding forces modeled using nonlinear viscoelastic impact model – developed in this paper using an explicit time integration method estimated the peak values of the pounding force in the first and second collision at 922 kN and 4070 kN, respectively. One would judge the apparently big difference in the estimated pounding forces, but figure 7 shows that the transferred momentum for the first collision, in any of the four previously discussed subchapters is comparable, as tabulated in table 5.

Table 5

Transferred linear momentum for the first collision

2 SDOF: Pounding model	Transferred linear momentum
Stereomechanics: linear behavior	$H_{linear}^{stereo} = 36.07 \text{ kN} * \text{s}$
Stereomechanics: Nonlinear behavior	$H_{nonlin}^{stereo} = 31.653 \text{ kN} * \text{s}$
Nonlinear viscoelastic impact element: linear behavior	$H_{linear}^{nonlin visco} = 28.77 \text{ kN} * \text{s}$
Nonlinear viscoelastic impact element: Nonlinear behavior	$H_{nonlin}^{nonlin visco} = 24.35 \text{ kN} * \text{s}$

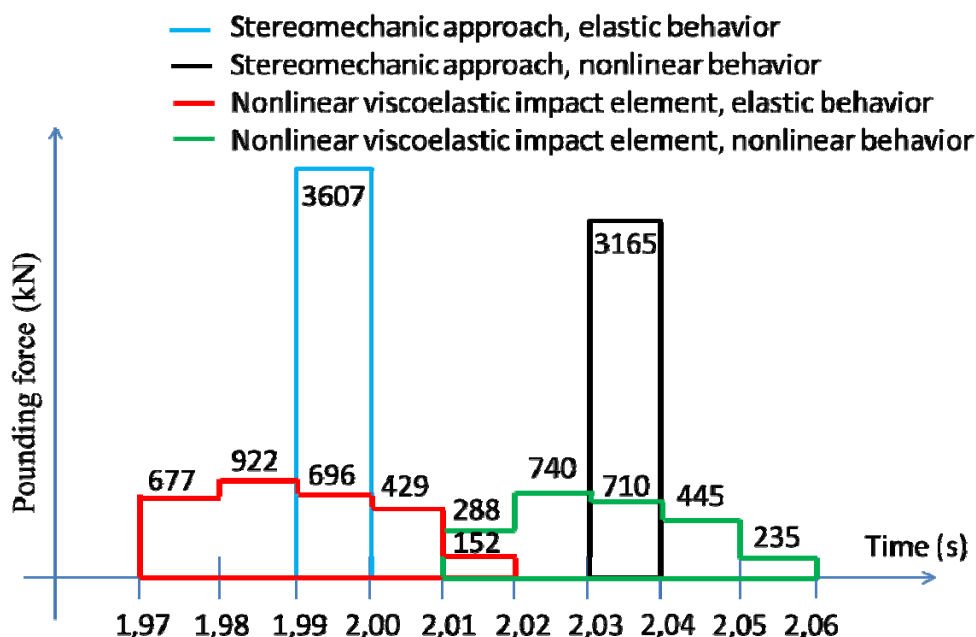
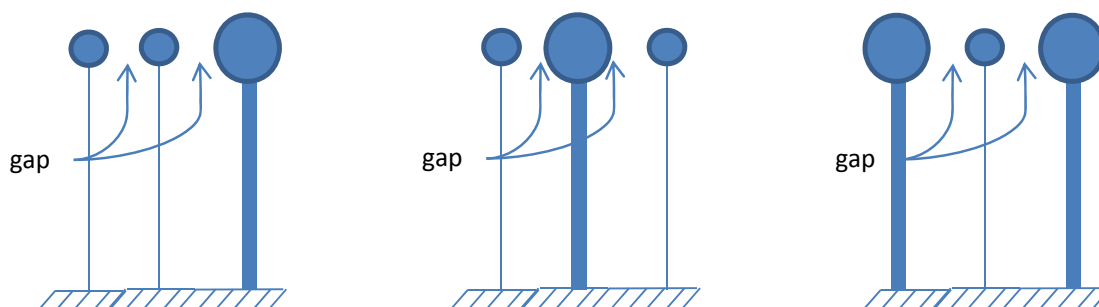


Fig. 7 - Pounding force for the first collision obtained in the described models

4. Structural pounding between three adjacent structures

The second part of this study addresses the pounding effect considering configurations of three structures with more or less different dynamic characteristics, located adjacent one to another. The previously discussed models are further investigated in three buildings layout patterns illustrated in figure 8, which simulate the most common type of layout typically found in cities.



Layout A: Stiff structure located at the edge of the array

Layout B: Stiff structure located in the middle of the array

Layout C: Weak structure located in the middle of the array

Fig. 8 - Typical structural layout found in modern cities

4.1. Linear and nonlinear response using stereomechanics approach

Both linear and nonlinear behavior of the structures is accounted using the stereomechanics approach to investigate the pounding forces obtained in the three layouts depicted in figure. 8. Figure 9, 10 and 11 illustrates the displacement time history and pounding forces for layout A, B and C respectively. The values of the transferred linear momentum in all the investigated scenarios are tabulated in table 6. Pounding forces tables with values are no longer included in this paper because of their table dimensions.

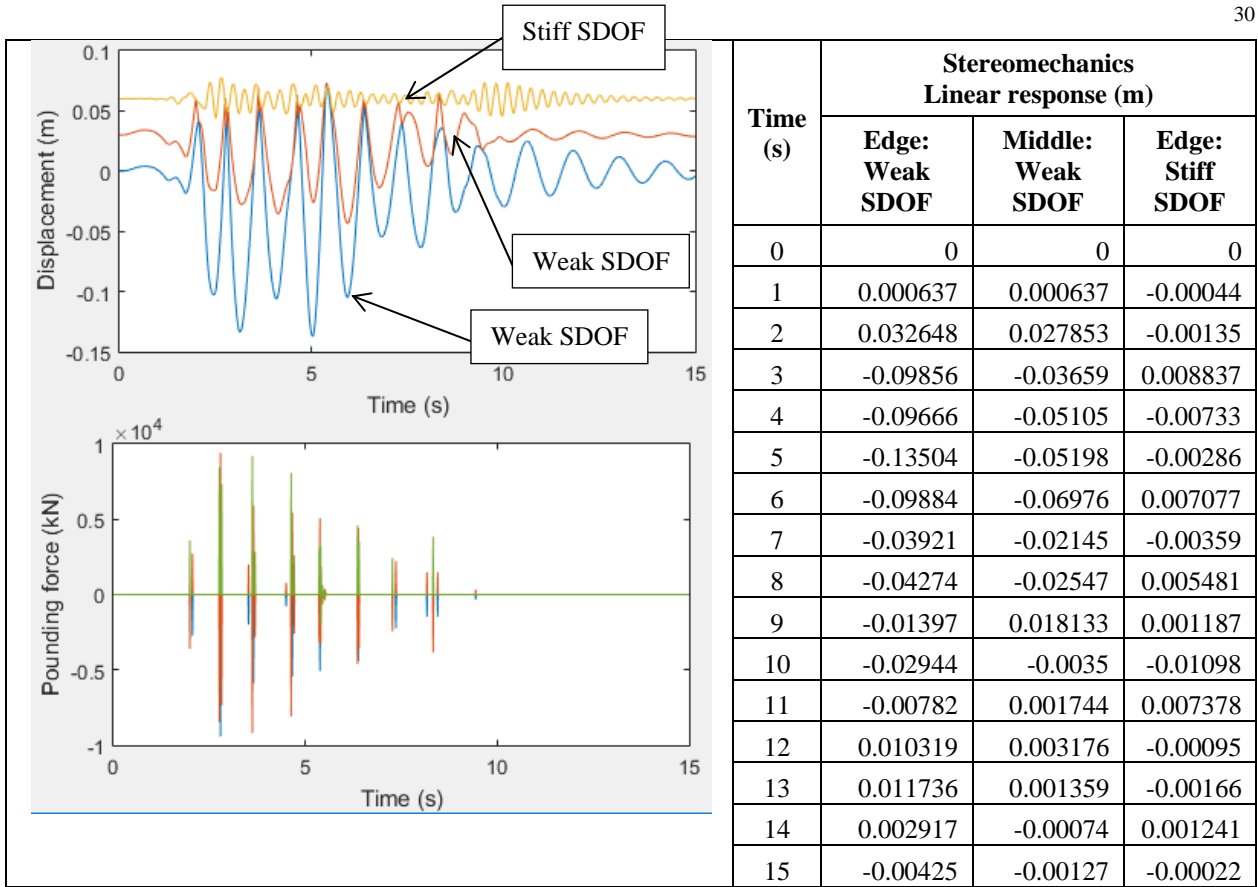


Fig. 9a - Stereomechanical impact: linear elastic time histories under the first 10 s of the NS component of the El Centro recording for layout A

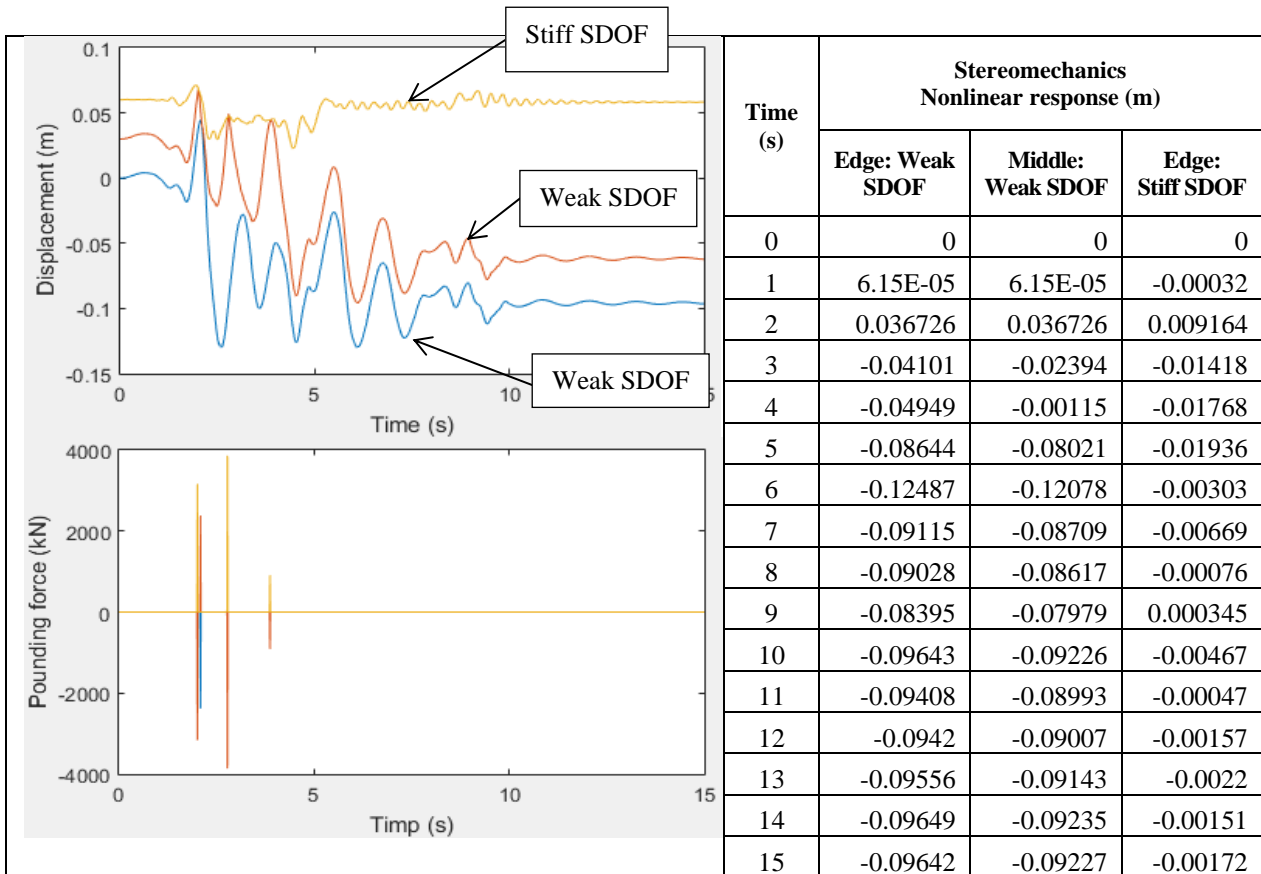


Fig. 9b - Stereomechanical impact: nonlinear time histories under the first 10 s of the NS component of the El Centro recording for layout A

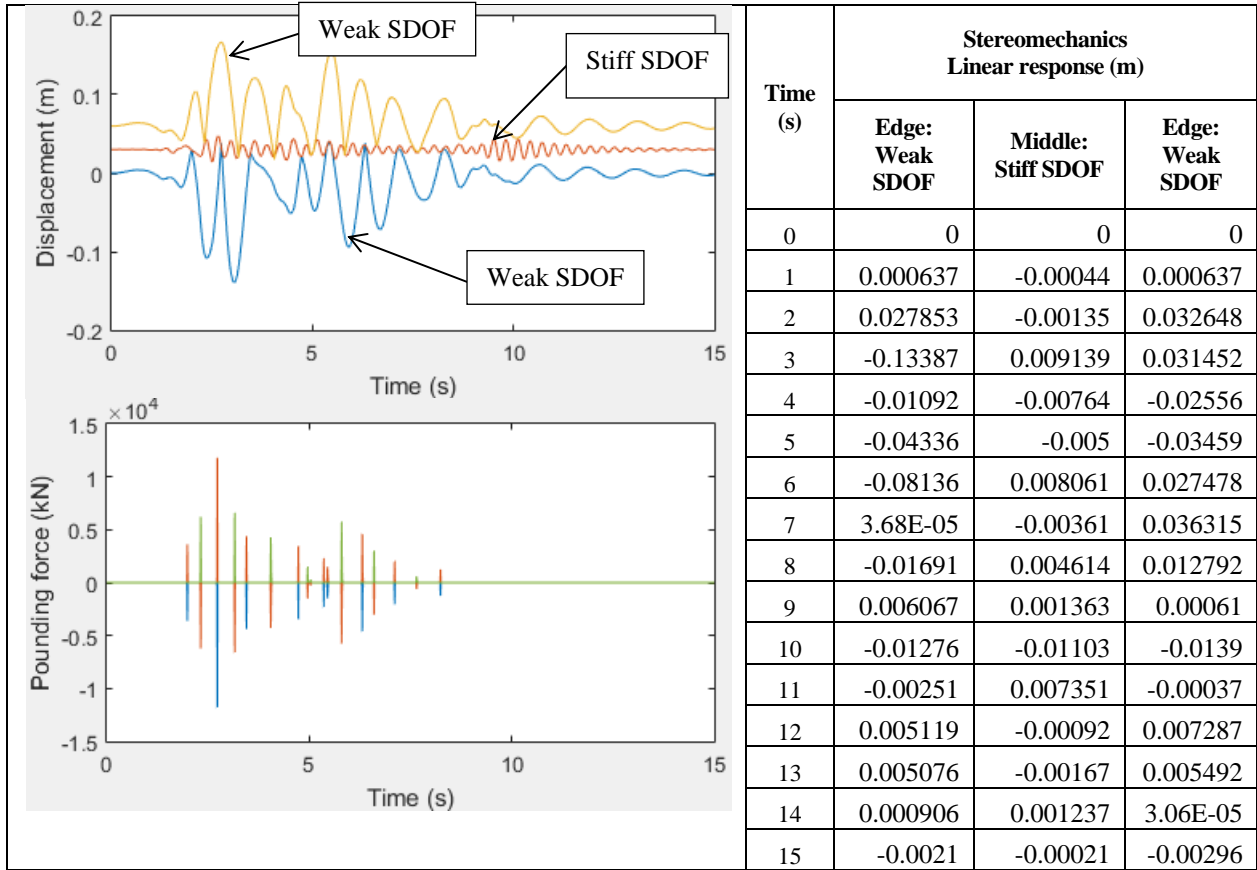


Fig. 10a - Stereomechanical impact: linear elastic time histories under the first 10 s of the NS component of the El Centro recording for layout B

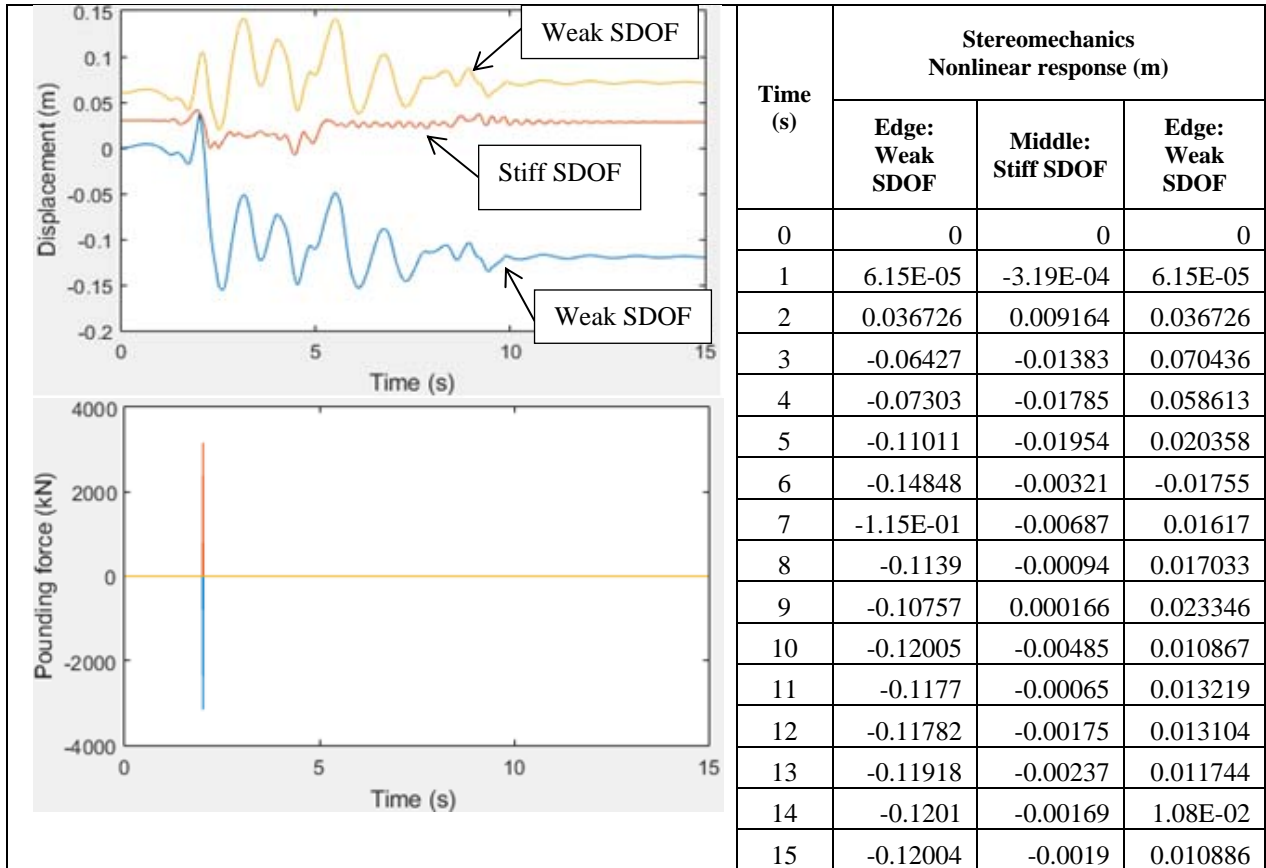


Fig. 10b - Stereomechanical impact: nonlinear time histories under the first 10 s of the NS component of the El Centro recording for layout B

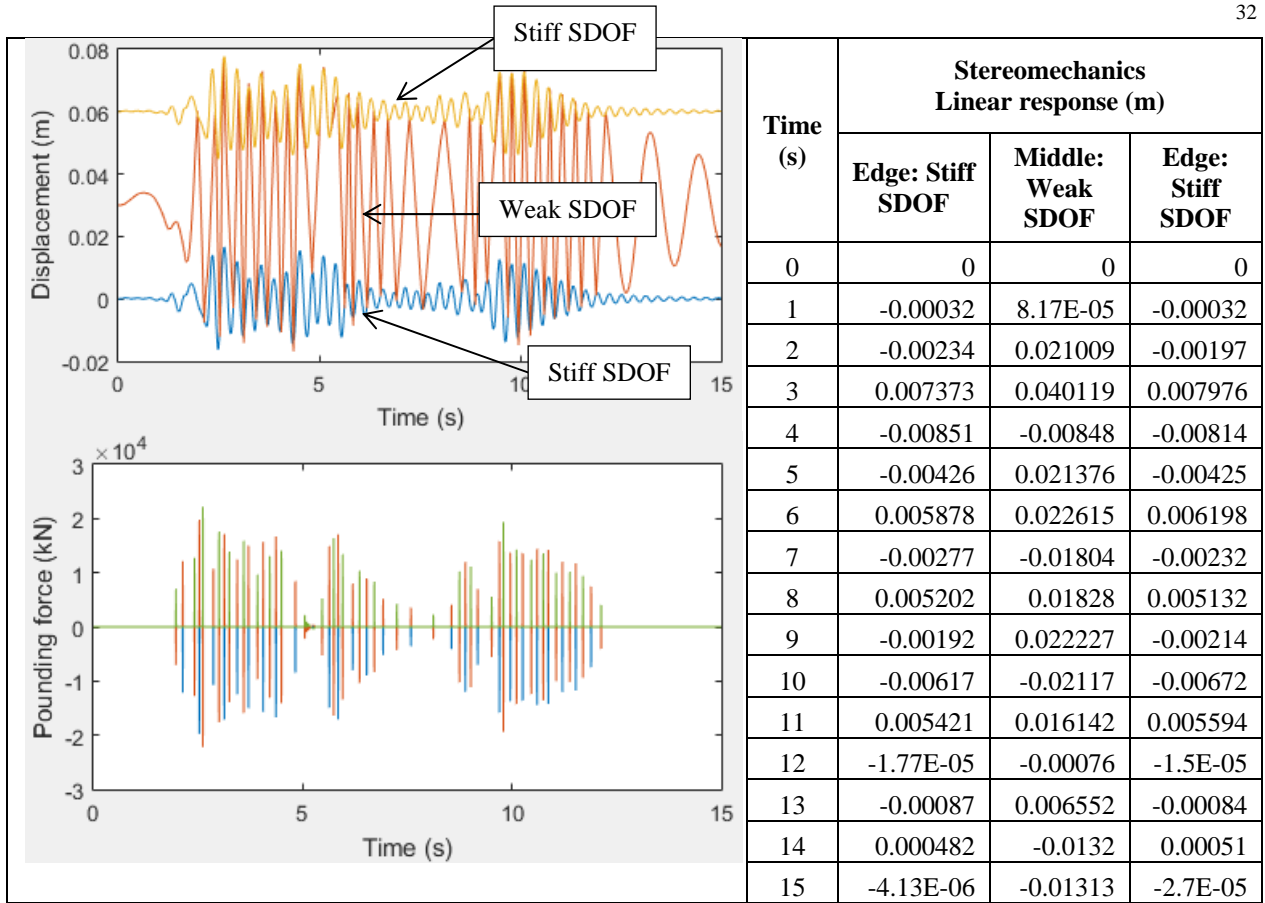


Fig. 11a - Stereomechanical impact: linear elastic time histories under the first 10 s of the NS component of the El Centro recording for layout C

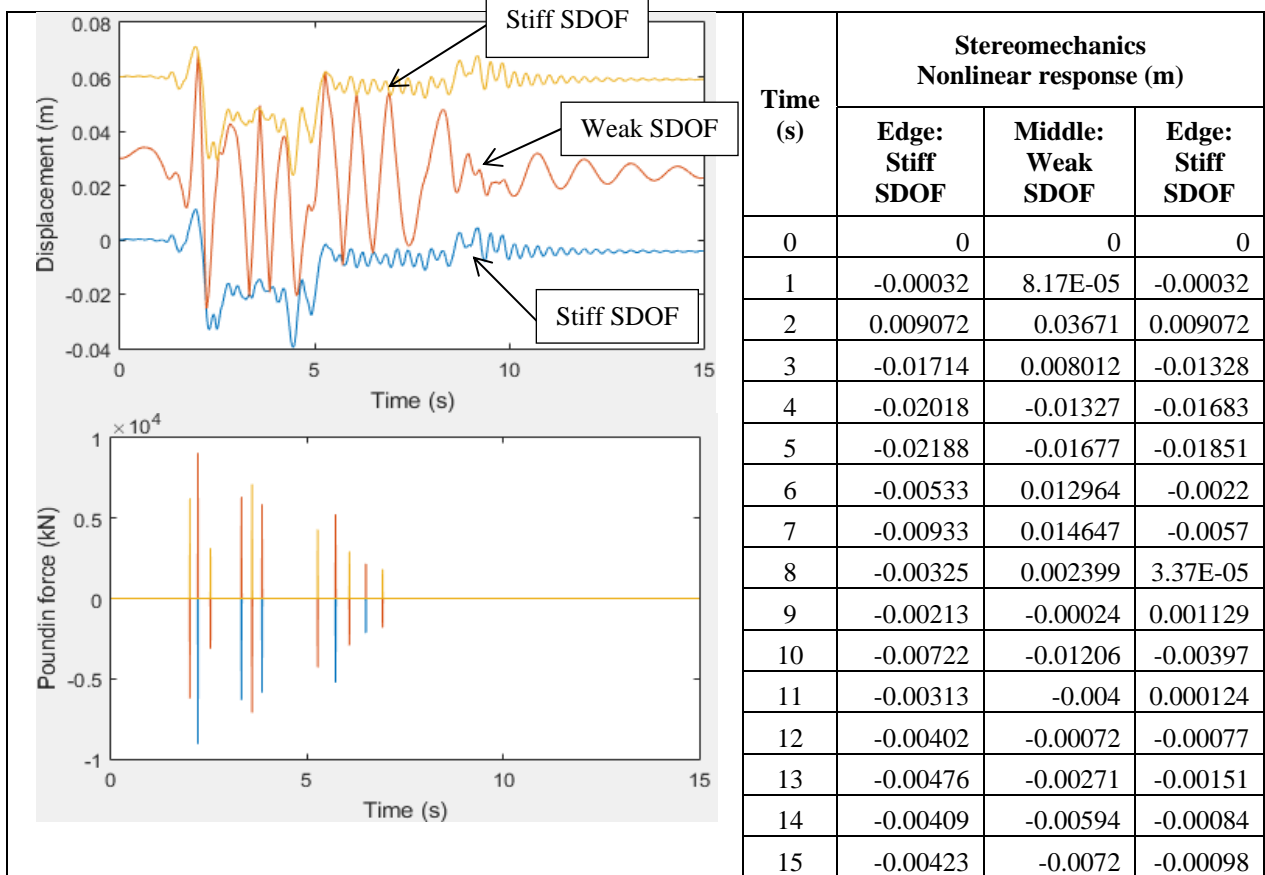


Fig. 11b - Stereomechanical impact: nonlinear time histories under the first 10 s of the NS component of the El Centro recording for layout C

Stereomechanical approach: Transferred linear momentum in the analysed scenarios

Scenario	Timestep [s]	Analysis type	SDOF type	Trnsasferred linear momentum [$kN * s$]
Layout A	0,01	Stereomecal approach, elastic behavior of SDOF's	Weak SDOF	456,9
			Weak SDOF	1170,8
			Stiff SDOF	725,4
		Stereomecal approach, nonlinear behavior of SDOF's	Weak SDOF	23,79
			Weak SDOF	103,13
			Stiff SDOF	79,35
Layout B	0,01	Stereomecal approach, elastic behavior of SDOF's	Weak SDOF	366,44
			Stiff SDOF	671,69
			Weak SDOF	305,24
		Stereomecal approach, nonlinear behavior of SDOF's	Weak SDOF	31,63
			Stiff SDOF	31,63
			Weak SDOF	0
Layout C	0,005	Stereomecal approach, elastic behavior of SDOF's	Stiff SDOF	1694,6
			Weak SDOF	3397,0
			Stiff SDOF	1702,5
		Stereomecal approach, nonlinear behavior of SDOF's	Stiff SDOF	157,98
			Weak SDOF	291,79
			Stiff SDOF	133,80

Layout C numerical model needed adjustment at the time step ($\Delta t = 0,005 s$) because of the high gradient of the velocity associated with the weak SDOF located between two stiff SDOF's. Consequently, greater peak values for the pounding force are obtained in the elastic behavior analysis, while the transferred linear momentum remains the same. In the elastic analysis, for $\Delta t = 0,01 s$ one would obtain displacement values greater than the gap (the structures are tangling). The values of the transferred linear momentum tabulated in table 6 are in close relation with the analysis performed on two SDOF's only, namely lower values of the transferred linear momentum are obtained in the nonlinear analysis. This is due the lower number of collision and due the increase in nonlinear hysteretic energy.

4.2. Linear and nonlinear response using nonlinear viscoelastic impact element approach

The layouts previously described are further investigated using the nonlinear viscoelastic impact element. Figure 12, 13 and 14 illustrate the linear and nonlinear behavior of structures in the analyzed scenarios. The minor aparent tangling of the structures depicted in figures 12-14, which represent the deformation of the colliding bodies, are related to the nonlinear viscoelastic impact element, which is "smoothing" the value of the pounding force for several adjacent timesteps, as depicted in figure 7. In the case of linear behavior of SDOF's , comparing table 6 and table 7 data, one can observe that the stereomechanical approach leads to greater values of total transferred momentum. In the case in which nonlinear behavior of structures is considered, the same linear momentum is transferred. One conclusion is that both the peak value of the pounding force and the transferred linear momentum are important. The nonlinear viscoelastic impact element has the advantage of a better modeling of the pounding force time-history. The drawback of the the nonlinear viscoelastic impact element is that it is dependent of some material parameters that need to be found experimentally and numerically calibrated.

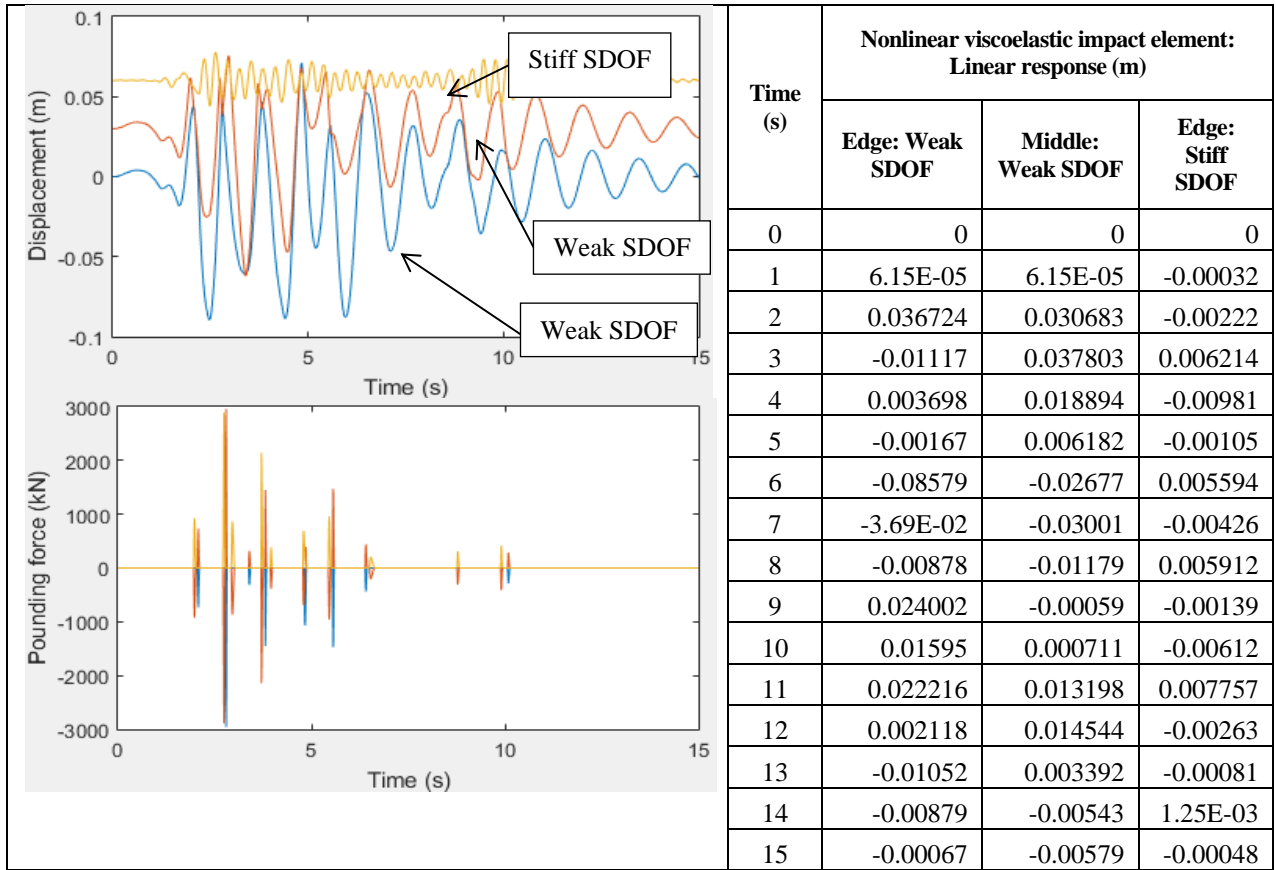


Fig. 12a - Nonlinear viscoelastic impact element: linear elastic time histories under the first 10 s of the NS component of the El Centro recording for layout A

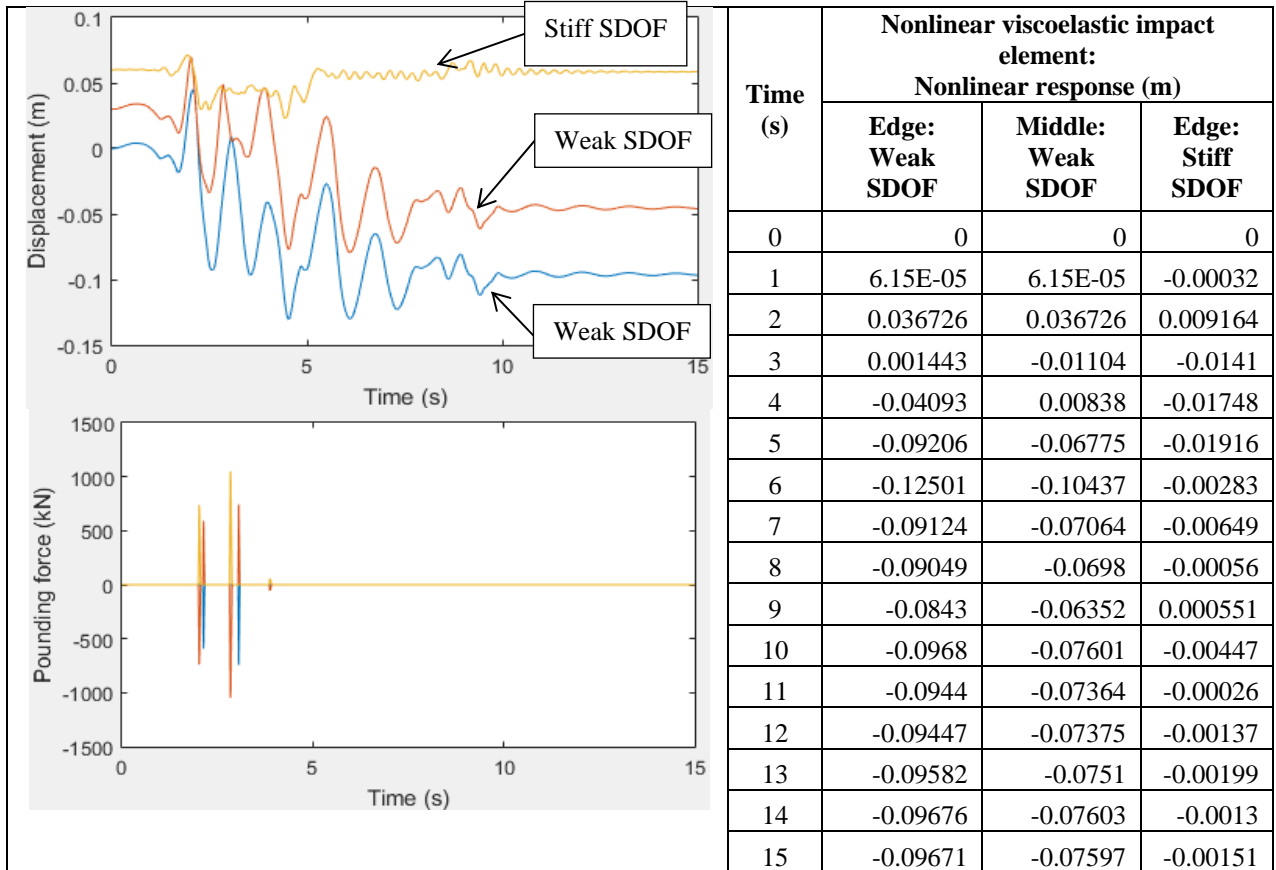


Fig. 12b - Nonlinear viscoelastic impact element: nonlinear time histories under the first 10 s of the NS component of the El Centro recording for layout A

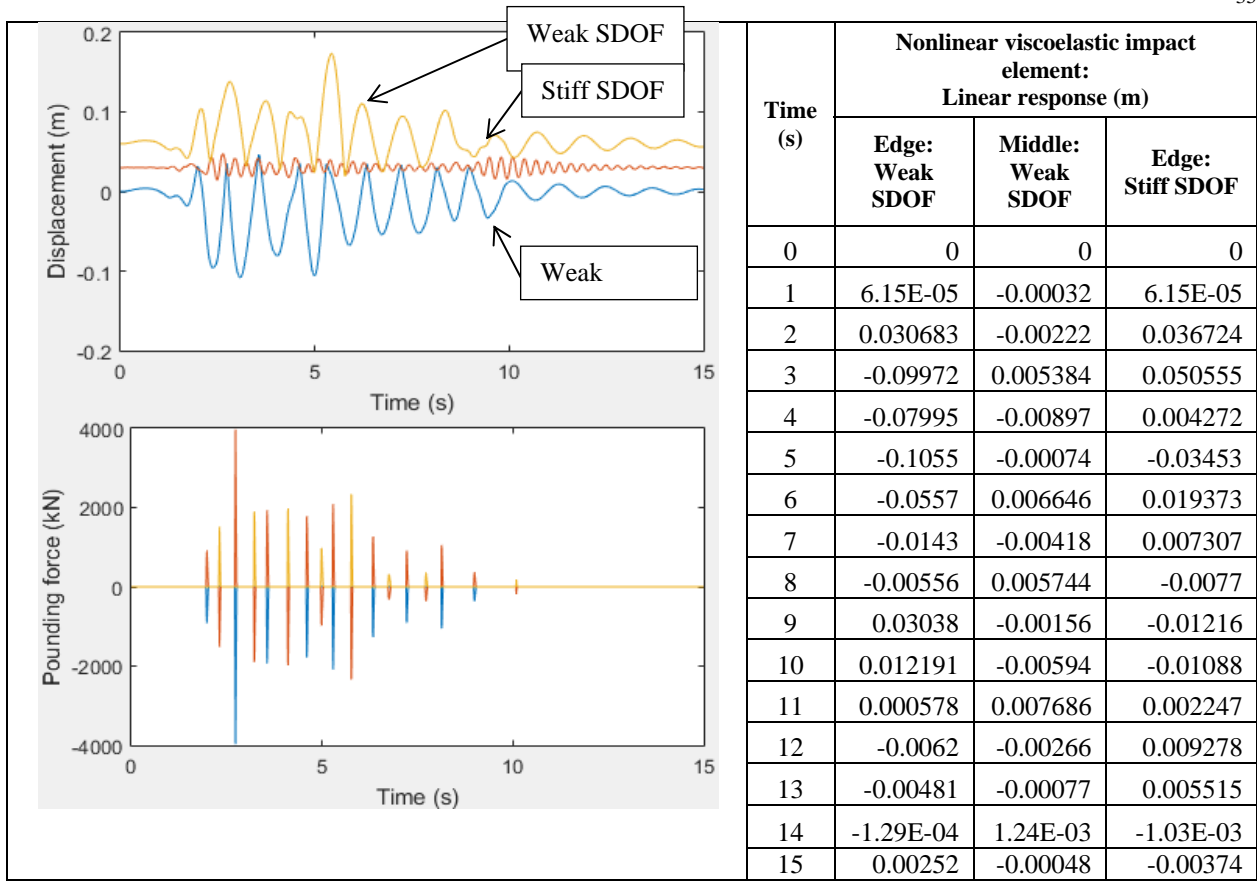


Fig. 13a - Nonlinear viscoelastic impact element: linear elastic time histories under the first 10 s of the NS component of the El Centro recording for layout B

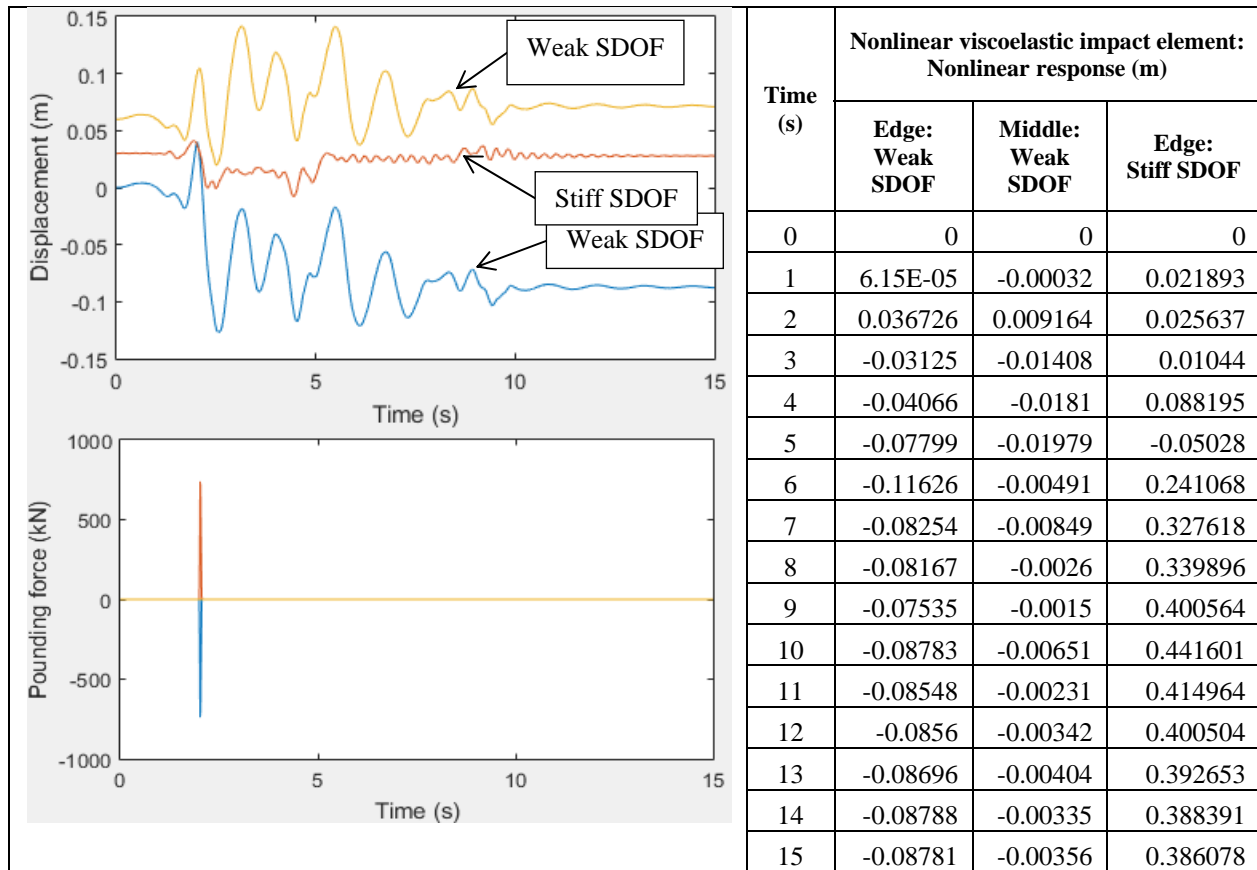


Fig. 13b - Nonlinear viscoelastic impact element: nonlinear time histories under the first 10 s of the NS component of the El Centro recording for layout B

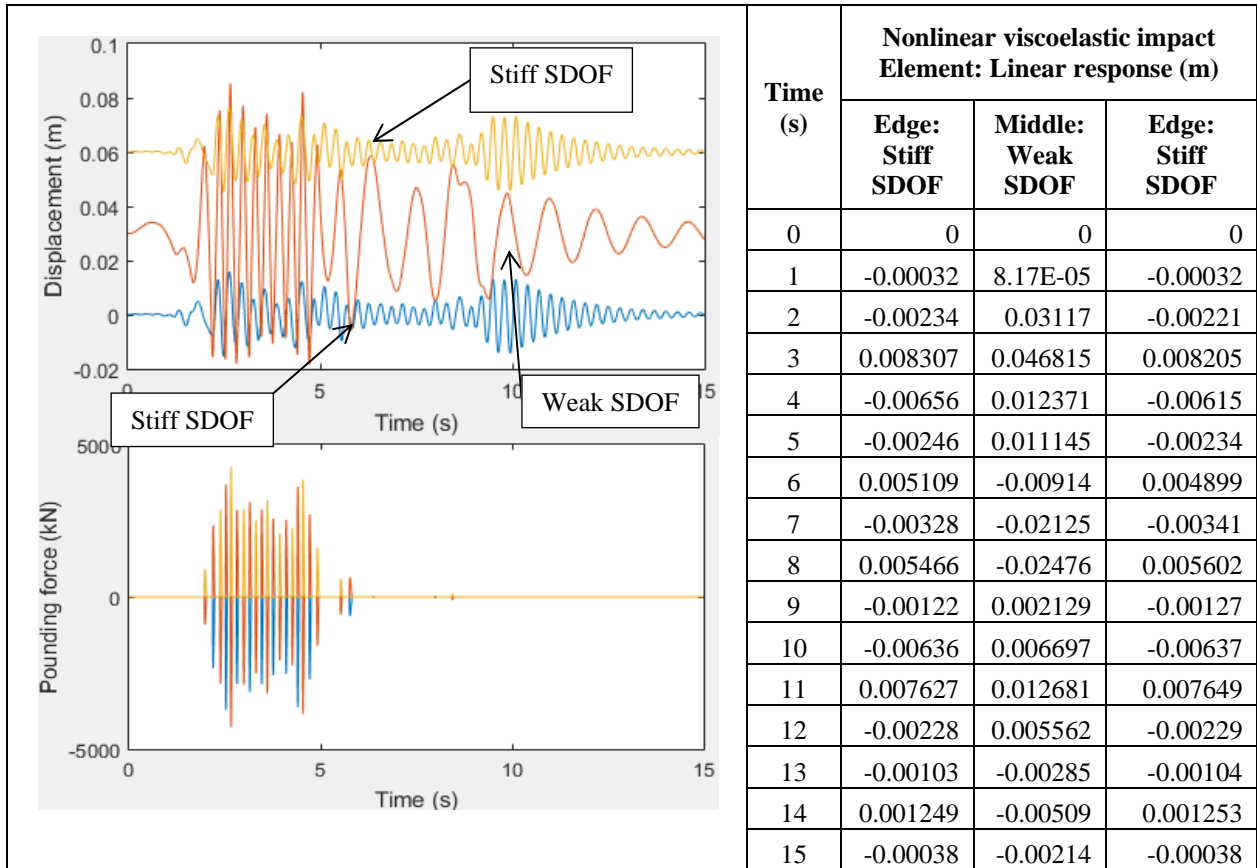


Fig. 14a - Nonlinear viscoelastic impact element: linear elastic time histories under the first 10 s of the NS component of the El Centro recording for layout C

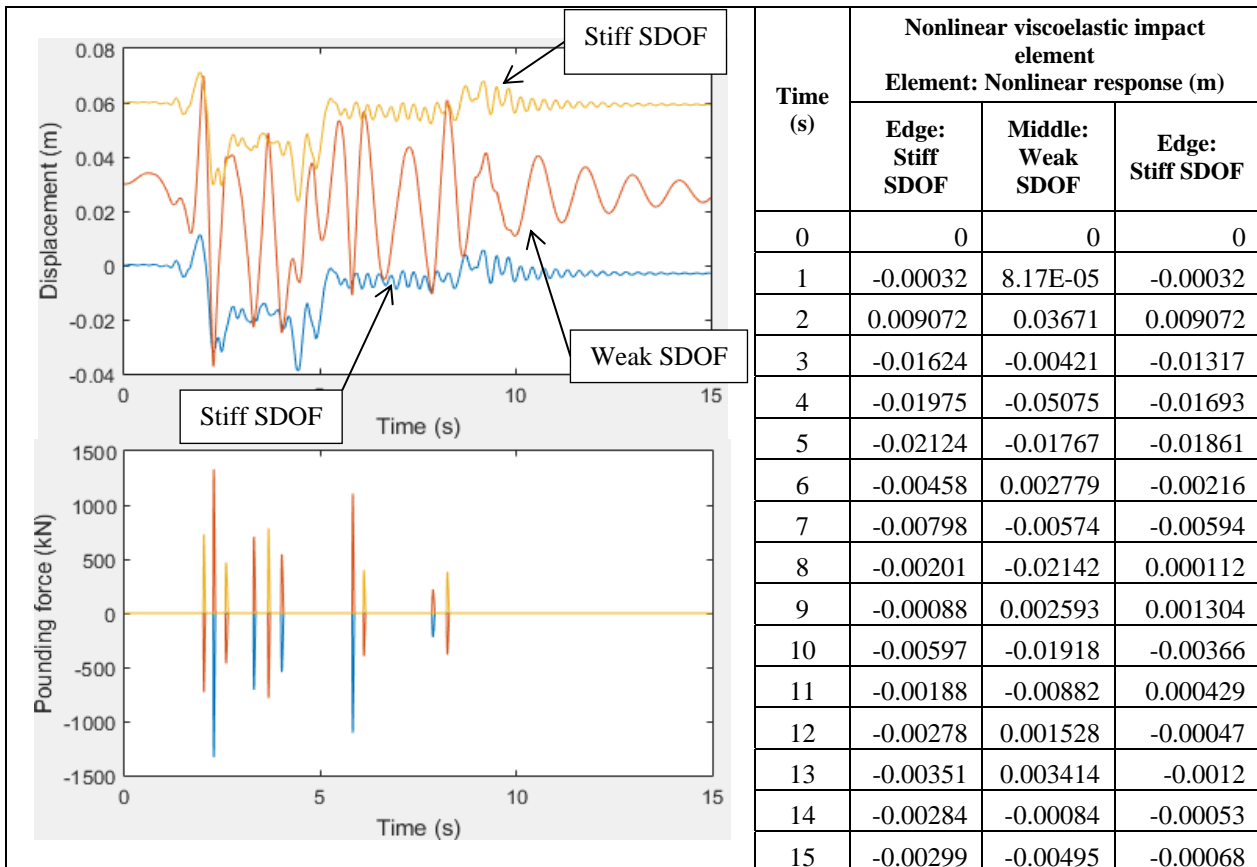


Fig. 14b - Nonlinear viscoelastic impact element: nonlinear time histories under the first 10 s of the NS component of the El Centro recording for layout C

Nonlinear viscoelastic impact element approach: Transferred linear momentum in the analysed scenarios

Scenario	Δt [s]	Analysis type	SDOF type	Transferred linear momentum [kN * s]
Layout A	0.01	Nonlinear viscoelastic impact element, Elastic behavior of SDOF's	Weak SDOF	207,06
			Weak SDOF	467,27
			Stiff SDOF	293,93
		Nonlinear viscoelastic impact element, nonlinear behavior of SDOF's	Weak SDOF	32,01
			Weak SDOF	93,55
			Stiff SDOF	61,54
Layout B	0,01	Nonlinear viscoelastic impact element, Elastic behavior of SDOF's	Weak SDOF	409,71
			Stiff SDOF	681,92
			Weak SDOF	272,20
		Nonlinear viscoelastic impact element, nonlinear behavior of SDOF's	Weak SDOF	24,35
			Stiff SDOF	24,35
			Weak SDOF	0
Layout C	0,005	Nonlinear viscoelastic impact element, Elastic behavior of SDOF's	Stiff SDOF	811,4
			Weak SDOF	1628,6
			Stiff SDOF	817,2
		Nonlinear viscoelastic impact element, nonlinear behavior of SDOF's	Stiff SDOF	142,66
			Weak SDOF	243,64
			Stiff SDOF	100,98

4.3 Discussion of the results

Comparing table 6 and table 7 data, one can observe that the stereomechanical approach leads to greater values of total transferred momentum in the case of linear behavior of SDOF's. In the case in which nonlinear behavior of structures is considered, the same linear momentum is transferred. One conclusion is that not only the peak value of the pounding force is important, but also the transferred linear momentum. Consequently, the stereomechanical approach gives a fast and clear view of the collision time and transferred momentum, with the drawback of overestimating the peak value of the pounding force. The nonlinear viscoelastic impact element has the advantage of a better modeling of the pounding force time-history, with the drawback of being dependent of some material parameters that need to be found experimentally and numerically calibrated.

Layout C, in which a weak structure is located between two structures, led to a decrease of the nonlinear incursions compared with the case in which the same structure can deform free. The stiff structures act like elastic restraints, causing the structure behave more "elastic", and to transfer the energy induced by the earthquake to the adjacent stiff structures. Fig. 15 illustrates the shear force time-history for the weak structure, in the case of Layout C compared to the case in which no collision is considered.

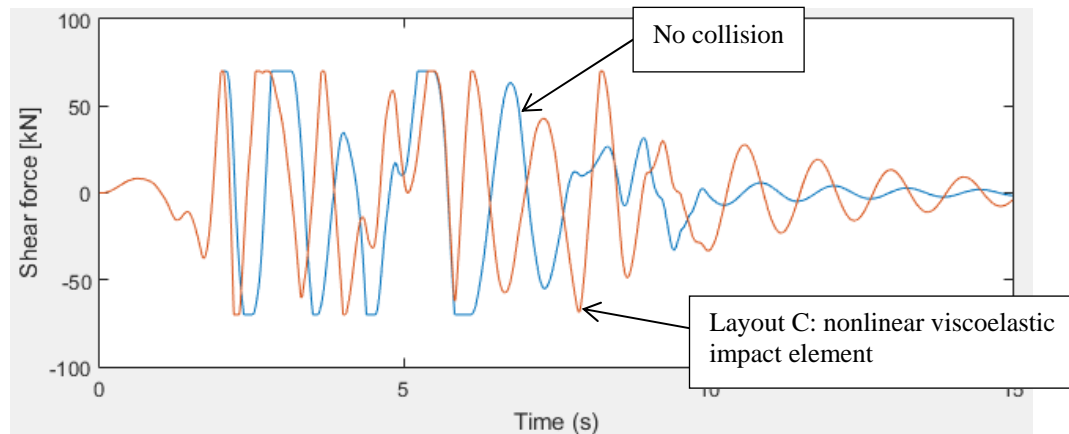


Fig. 15 - Weak structure shear force time history: comparison between the case no pounding is considered and Layout C

5. Conclusions

In this paper the pounding forces are modeled using the stereomechanics approach and using the nonlinear viscoelastic impact element. An explicit the time integration method is used. In the first part of the paper structural pounding is modeled using a stereomechanics approach which relies on the conservation of momentum between masses. To that extent the authors developed a routine in MATLAB which has been validated with results from reference [7]. Although sound from a theoretical point of view, the stereomechanics approach does not model the pounding effect consistently as it implies that the pounding force between the two masses acts in a small interval of time. Also, the magnitude of the force is high as the conservation of momentum acts specifically in the time step when the collision is detected.

The study also addresses pounding while considering the nonlinear response of the SDOF structures. In the first part of the study the linear and the nonlinear pounding of the considered models is studied. For the studied case, the number of collisions between the structures is higher for the elastic models than for the nonlinear ones. Thus at the first moment of pounding the weak structure suffers a significant displacement which is amplified in the nonlinear domain, and cannot be recovered during subsequent oscillations.

Chapter 3 of the study, implements a nonlinear viscoelastic impact element which models more accurately the pounding effect. The result is a significant decrease of the peak value of the pounding forces with respect to the stereomechanical model. Although the pounding force is reduced by an order of magnitude, the transferred momentum suffers only a slight reduction of about 20%. The nonlinear model is far more effective at modeling peak values of the pounding forces, but implies the use of experimental data to obtain the parameters involved.

In chapter 4, the article investigates different layouts of 3 structures, varying the stiffness of the SDOFs. From the point of view of maximum displacement, the least favorable case is the one with a stiff structure placed between two weak structures. The conclusions are based on only one ground motion recording with specific frequency content.

The research in the article can be continued by considering the directionality effect of the earthquake. For all of the structures the earthquake was considered as acting from left to right. A reversed directivity of the earthquake which is highly plausible due to the variability of the layout of the structures related to the fault would produce different results. The effect of different frequency content recordings may be investigated in future work. While the model investigated in this study can be directly applied to single story structures, a MDOF model would represent more accurately the effect of pounding on regular structures.

References

- [1] Anagnostopoulos, S. A. (1988). Pounding of buildings in series during earthquakes. *Earthquake Engineering and Structural Dynamics*. 16, 443-456.
- [2] Mate N. U., Bakre S. V., Jaiswal O. R. (2012). Comparative Study of Impact Simulation Models for Linear Elastic Structures in Seismic Pounding. *Proceedings of the fifteenthth world conference on earthquake engineering*. Lisbon, Portugal
- [3] Mate N. U., Bakre S. V., Jaiswal O. R. (2014). Seismic pounding of adjacent linear elastic buildings with various contact mechanisms for impact simulation. *Asian journal of civil engineering*. vol. 16, no. 3, 383-415
- [4] Jankowski R. (2004). Non-linear viscoelastic model of structural pounding. *13th World Conference on Earthquake Engineering Vancouver*, Canada. Paper No. 3082
- [5] Mahmoud S., Jankowski R. (2011). Modified Linear Viscoelastic model of earthquake-induced structural pounding. *IJST, Transactions of Civil and Environmental Engineering*. Vol. 35, 51-62
- [6] Jankowski R. (2007). Theoretical and experimental assessment of parameters for the non-linear viscoelastic model of structural pounding. *Journal of theoretical and applied mechanics*. Vol. 4, 931-942
- [7] Jankowski R., Mahmoud S. (2015) *Earthquake-Induced Structural Pounding*. Switzerland: Springer International Publishing.
- [8] Salam S. A., Eraky A., Mottaleb H. A., Abdo A. (2015). Pounding Control of Structures Using Base Isolation. *International Journal of Engineering and Innovative Technology (IJEIT)*. Vol. 4, Issue 9, 171-177
- [9] Barros R. C., Khatami S. M. (2012). Seismic Response Effect of Shear Walls in Reducing Pounding Risk of Reinforced Concrete Buildings Subjected to Near-Fault Ground Motions. *Proceedings of the fifteenth world conference on earthquake engineering*. Lisbon, Portugal
- [10] Polycarpou P., Komodromos P. (2013) On the numerical simulation of structural pounding in three Dimensions. *World Congress on Advances in Structural Engineering and Mechanics (ASEM13)*, Jeju, Korea
- [11] Yang Y. , Li S., Xie L. (2008). Research on collision of beam-type structures based on hertz-damp model , *The 14 th World Conference on Earthquake Engineering*, Beijing, China
- [12] Efraimiadou S., Hatzigeorgiou G. D., Beskos D. E. (2012). Structural pounding between adjacent buildings: The effects of different structures configurations and multiple earthquakes. *Proceedings of the fifteenth world conference on earthquake engineering*. Lisbon, Portugal
- [13] Arpitha K, Umadewi R., (2016). Effect of seismic pounding between reinforced concrete buildings. *International Journal of Latest Trends in Engineering and Technology (IJLTET)*. Vol. 7 issue 2, 576-583
- [14] Raheem S. E. A. (2006). Seismic Pounding between Adjacent Building Structures. *Electronic Journal of Structural Engineering*. Vol. 6, 66-74
- [15] Ehab M., Salem H., Mostafa H., Yehia N. (2014). Earthquake Pounding Effect on Adjacent Reinforced Concrete Buildings. *International Journal of Computer Applications*. Vol. 106 ,No.9, 27-34
- [16] Chopra A.K. (2007). *Dynamics of structures*. Pearson Education,
- [17] Goldsmith W. (1960). *Impact. The Theory and physical behavior of colliding solids*. London: Edward Arnold LTD